Optimal unidirectional generation of a dispersive wave mode with dual-array transducer

Alan C. Kubrusly[a], Lei Kang[b], Steve Dixon[c]

[a]*Centre for Telecommunication Studies, Pontifical Catholic University of Rio de Janeiro, Rio de Janeiro, Brazil*
[b]*School of Energy and Electronic Engineering, University of Portsmouth, Portsmouth, PO1 3DJ, UK*
[c]*Department of Physics, University of Warwick, Coventry, CV4 7AL, UK*

Abstract

Array transducers are commonly used to generate several types of waves, such as ultrasonic guided waves. They consist of a series of periodic wave source elements, and thus define a nominal or dominant wavelength of generated waves. A common approach to generating waves in a single direction is to use two identical wave sources, or two arrays of sources forming a dual-array transducer, that are separated by a quarter wavelength. Then, one source is activated a quarter of a time period after the other. In this way, constructive interference arises in one direction, whilst destructive interference arises in the opposite direction, making the total wave source unidirectional. This principle assumes that the frequency content of the generated wave is monochromatic. When there is some frequency bandwidth to the wave generated, such as with finite-length pulses, one cannot satisfy simultaneously constructive and destructive interference in opposite directions with dual-array transducers. For a non-dispersive wave mode, ideal destructive interference for pulsed waveform is obtained if one of the sources is inverted relative to the other, so that, in theory, complete cancellation can be achieved. Moreover, most guided wave modes are dispersive, meaning that, different frequencies propagate at different phase speeds. This limits the amount of wave cancellation in one direction and constructive interference in the other. Here, we describe the operation of the dual-array transducer in the frequency-wavenumber domain and use it to propose two new excitation methods, based on a frequency-dependent phase-shift strategy, that is designed through the dispersion relationship of the wave mode of interest. These provide ideal constructive or destructive interferences for dispersive waves, and achieve optimal unidirectional generation behaviour for dispersive wave modes. The new methods were experimentally assessed with shear-horizontal ultrasonic waves, generated by a dual periodic

Email addresses: alan@cpti.cetuc.puc-rio.br (Alan C. Kubrusly), lei.kang@port.ac.uk (Lei Kang), S.M.Dixon@warwick.ac.uk (Steve Dixon)

permanent magnet electromagnet acoustic transducer. The optimal excitation signal yielded up to 30 dB unidirectionality, when generating the dispersive SH1 wave mode in an aluminium plate.
Keywords: dual-array transducers, frequency-wavenumber domain, unidirectional wave generation, dispersive ultrasonic wave, electromagnet acoustic transducer.

1. Introduction

Array or comb transducers are composed of several wave source elements being widely used to generate and receive several types of ultrasonic waves such as surface waves [1, 2], Lamb [3–5] or shear horizontal (SH) [6–8] waves in plates, or guided waves in rods and pipes [9, 10]. They are typically made of piezoelectric elements [11–13] or electromagnetic-acoustic transducers (EMATs) [5, 14]. Some types of EMATs impose their stimuli in the medium naturally forming an array, such as meander-line EMATs [15–17] or periodic permanent magnet (PPM) [18, 19]. In the former, the coil is periodically wound with its spatial period imposing the nominal wavelength of the generated wave [16], being often used to generate Rayleigh or Lamb waves. The latter generates SH waves and also imposes the nominal or dominant wavelength, but this is determined by the spacing of the magnets in the array of magnets, and is not imposed by the coil [19, 20].

Array transducers generate waves that propagate both forwards and backwards [21]. Depending on the application, this can be an undesirable characteristic. For instance, in non-destructive evaluation of plates and pipes, the backward propagated wave can be reflected and mixed with the wave mode of interest, producing complex received signals [22]. Unidirectional generation can be achieved through the interference mechanism. For instance, if sources positioned along the propagation direction are excited with phased pulses [3, 9, 23]. This can be achieved with phased array transducers, where the pulse applied to each array element can be controlled independently. This allows a great wave generation control, such as direction and wavelength regulation [4, 5]. Phased arrays, however, require a multichannel emitting circuitry in order to independently control each element. Unidirectional generation can be achieved in a simpler manner with array transducers formed by only two independent channels, comprising a so-called dual-array transducer, using two time-delayed pulses [7, 15, 24–27].

Dual-array transducers were used previously to generate different types of guided waves. Wang et al. [15] generated Lamb or shear vertical waves unidirectionally with a dual meander-line coil EMAT separated by a quarter wavelength. Recently Rieger et al.[27] generated a Lamb wave mode unidirectionally with a coil-only EMAT, without a permanent magnet. SH wave can also

be generated unidirectionally relying on this principle, as used by Chen et al. [7] who utilised thickness-shear mode piezoelectric strips. We recently presented two designs of dual PPM EMATs that generated the non-dispersive fundamental SH0 mode in a single direction, namely a dual side-shifted PPM array [25] and a PPM array with a dual-linear coil [26], instead of the conventional racetrack coil.

Using time-delayed excitation signals allows one to obtain ideal constructive or destructive interference with a dual-array transducer. This principle relies on applying a time-delayed excitation signal to one array in which the delay matches the time it takes for the wave to propagate from one array to the other. For monochromatic signals, this provides both constructive interference in one direction and destructive in the opposite direction. In practical terms, however, the driving signal is finite-length and has some frequency bandwidth. In this case, the waves generated from both arrays combine perfectly constructively when propagating in one direction, whilst the wave that propagates in the other direction suffers a partial destructive interference presenting considerably lower amplitude, but are not completely cancelled. In addition to a time delay, if one of the exciting pulses is inverted, that is, multiplied by -1, then the waves generated from both arrays are perfectly aligned in one direction but have opposite signs, therefore providing ideal perfect destructive interference [23]. These types of excitation signals' pairs can only provide theoretical perfect destructive or constructive interference for non-dispersive waves, whose wavenumber and frequency present a linear relationship, but is not ideal for dispersive waves.

In this paper, we exploit the frequency-wavenumber spectrum of dual-array transducers, in order to design excitation signals that provide ideal interference for dispersive waves, and optimize the unidirectional generation of dispersive waves. Next, we evaluate the proposed optimal excitation signals with SH ultrasonic guided waves, generated by a dual PPM EMAT in plates. Despite the motivation and evaluation of this work being the optimal generation of a dispersive SH wave mode in a single direction, the design mechanism holds for waves of any nature that are efficiently generated with array transducers; therefore, the theoretical derivation is presented here in a generic fashion. The rest of the paper is organized as follows. Section 2 defines the excitability of a wave generated by a dual-array transducer relying on the frequency-wavenumber spectrum and dispersion relationship of the wave of interest. Section 3 describes two methods that allow one to get ideal constructive or destructive interference for non-dispersive waves and two new methods that provide optimal interference for dispersive waves. Section 4 presents the basic principles of shear horizontal ultrasonic waves and the dual PPM-EMAT used for experimental

evaluation. Section 5 shows the experimental results and section 6 concludes the work.

2. Frequency-wavenumber spectrum analysis of dual array transducers

In order to analyse the wave generated by an array transducer, we assume that it can be modelled as a series of ideal waves sources that are periodically distributed in space and are driven by a time-domain signal common to all its elements. Each element is ideal in the sense that it is able to generate the wave of interest by imposing, through some physical coupling mechanism, an adequate stimulus and polarization. For example, it could be the induced force of an EMAT [28] or piezoelectric [29] transducer, polarized in order to generate the wave mode of interest.

Let $h_0(x)$ be the array spatial distribution that dictates the source's spatial distribution along the longitudinal coordinate, x, of a single array transducer. Fig. 1(a) exemplifies an ideal single array, where each element acts as a homogeneous source along its active length, m, with positive or negative polarity indicated by the plus or minus sign, respectively. Therefore, the spatial distribution $h_0(x)$ is given by the square-wave function shown in Fig. 1(b), which is centred at the origin of the x-axis. Since the array is composed of alternate-polarity sources [16], the separation between consecutive elements defines the half spatial period of the array, given by $\lambda/2 = m + g$, where g is the gap between areas of active length. The spatial period of the array defines the nominal wavelength, λ, of the waves that are generated predominately [19]. However, since the array is finite, in this example of three cycles, there exists a bandwidth of generated wavelengths given by the Fourier transform of $h_0(x)$:

$$H_0(\kappa) = \mathscr{F}\Big\{h_0(x)\Big\} \quad , \tag{1}$$

where κ is the spatial angular frequency, or the wavenumber. Fig. 1(c) shows the respective spatial spectrum. Note that it is centred around the nominal wavelength of the array.

The array is driven by a time-domain pulse, which can represent, for instance, the voltage applied to the elements of a piezoelectric array or the current injected into the coil of an EMAT. This pulse defines the temporal dependence of the transducer, here referred to as $g_0(t)$. Its Fourier transform provides the transducer's temporal spectrum:

$$G_0(\omega) = \mathscr{F}\left\{g_0(t)\right\} \quad , \tag{2}$$

where ω is the angular frequency. Fig. 2 and Fig. 3 exemplify pulses formed by an 8-cycle tone-burst pulse with centre frequency 258.3 kHz, and a 15-cycle tone-burst pulse with centre frequency

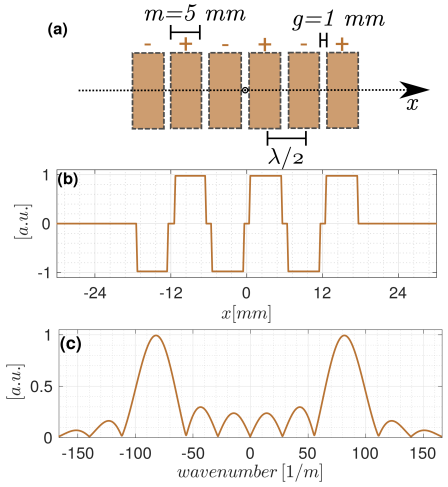

Figure 1: Schematic representation of an array transducer (a) composed of 3 periods of alternate polarity (pulse and minus signs) elements with active length m = 5 mm and the gap between elements g = 1 mm, thus providing a λ = 12 mm spatial period. Ideal transducer spatial profile (b) and the absolute value of its spatial spectrum (c).

577.7 kHz, respectively. In both cases, pulses were modulated by a Hamming window, applied to reduce side lobes in their frequency spectra [30].

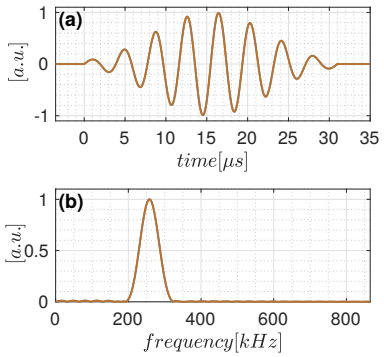

Figure 2: Excitation signal formed by an 8-cycle tone-burst pulse with centre frequency 258.3 kHz modulated by a Hamming window (a) and its frequency spectrum (b). The centre frequency matches the dispersion curve of the SH0 and at the nominal wavelength of the array, being thus adequate for generating this wave mode.

The combination, or the Cartesian product, of both temporal and spatial spectra provide the frequency-wavenumber spectrum of the transducer, or its operating region in the frequency-wavenumber plane, as follows:

$$S(\omega, \kappa) = G_0(\omega)H_0(\kappa) \quad . \tag{3}$$

Figures 4(a) and (b) show the operating region obtained from the spatial spectrum of Fig. 1(c) and

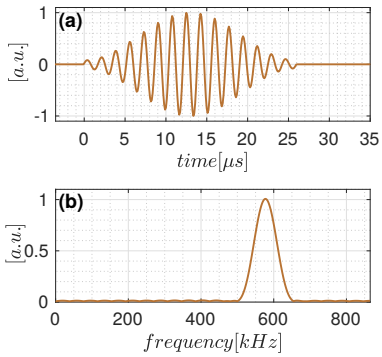

Figure 3: Excitation signal formed by a 15-cycle tone-burst pulse with centre frequency of 577.7 kHz modulated by a Hamming window (a) and its frequency spectrum (b). The centre frequency matches the dispersion curve of the SH1 guided wave modes at the nominal wavelength of the array, being thus adequate for generating this wave mode.

temporal spectra of Figs. 2(b) and 3(b), respectively. Note that it is centred at the centre frequency of the excitation signals and the centre wavenumber of the array, presenting a bandwidth in both axes.

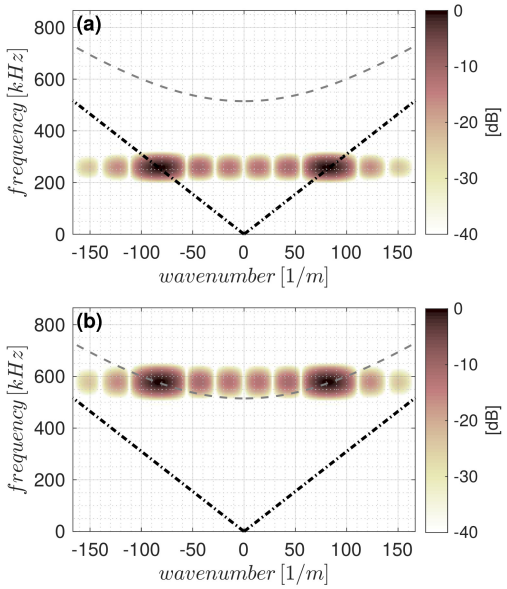

Figure 4: Operating region (colour plot) of a 3-cycle single-array transducer with 5 mm active length and 1 mm gap between active areas of the same array, thus producing a λ = 12 mm nominal wavelength, driven by (a) an 8-cycle tone-burst pulse with centre frequency of 258.3 kHz (shown in Fig. 2) and (b) 15-cycle tone-burst pulse with centre frequency of 577.7 kHz (shown in Fig. 3). The negative wavenumber axis is related to backward propagating waves. The black dash-dotted and grey dashed lines indicate the dispersion curve of the non-dispersive SH0 and dispersive SH1 modes, respectively, in a 3 mm thick aluminium plate.

The dispersion relationship of a wave relates its wavenumber to the frequency; in the ω-κ plane, the dispersion curve is the locus of wavenumber and frequency pairs that determine the wave propagation characteristics. A forward travelling wave presents a positive frequency wavenumber ratio, or its phase speed, c, whereas a backward travelling wave has a negative frequency wavenumber ratio. That is,

$$c = \pm\omega/\kappa \quad , \tag{4}$$

where the plus-minus symbol, $\pm$, corresponds to the direction of propagation, either forwards, plus sign, or backwards, negative sign. A non-dispersive wave presents a linear frequency-wavenumber relationship, or equivalently a constant phase speed, whereas a dispersive wave has a non-linear frequency-wavenumber relationship.

One can use the operating region and dispersion relationship of a given wave mode to design an adequate excitation signal and to predict the wave excitability. If the dispersion curve of a specific wave, which can be generated through the coupling mechanism of the chosen array, intersects $S(\omega, \kappa)$ at ω-κ values where its absolute value is high, this wave mode is generated predominantly [5, 16, 19, 20]. Therefore, the centre frequency of the excitation signal, $g_0(t)$, should be selected, via Eq. 4, in order to match the dispersion relationship of the wave mode of interest, at the nominal wavenumber imposed by the array. If a medium, however, supports several wave modes, then more than one mode can be simultaneously generated whenever several dispersion curves cross the operating region. One usually attempts to generate a single mode, which can be achieved by careful design of the operating region through the excitation signal or array geometry [8, 31].

In Fig. 4, superposed on $S(\omega, \kappa)$, there are two lines that represent the frequency-wavenumber relationship of possible propagating waves, or their dispersion curves. The black dash-dotted curve is a straight line meaning that this wave mode is non-dispersive, in contrast to the grey dashed curve, which is the dispersion curve of a dispersive wave mode with a non-linear frequency-wavenumber relationship. Note that, the high-amplitude spot of $S(\omega, \kappa)$ is crossed by the black or grey dispersion curves when the excitation signal is centred at 258.3 kHz [Fig. 4(a)] or 577.7 kHz [Fig. 4(b)], respectively, meaning that these wave modes are efficiently generated by the array at those frequencies. It is worth highlighting that, their temporal bandwidths are narrow enough so that the operating region only crosses the dispersion curve of the wave mode of interest, and it does not cross dispersion curves of the other wave mode, ensuring single-mode generation, in either case. Note that $S(\omega, \kappa)$ is symmetrical about the κ-axis, meaning that forward and backward

waves are generated with equal magnitude.

A dual-array system is composed of two arrays, $h_1(x)$ and $h_2(x)$, with the same shape as $h_0(x)$ but spaced by $\lambda/4$. Therefore, they can be expressed by $h_1(x) = h_0(x + \lambda/8)$ and $h_2(x) = h_0(x - \lambda/8)$. Consequently, in the wavenumber domain, one has

$$H_1(\kappa) = H_0(\kappa)e^{-j\kappa\lambda/8} \quad , \tag{5a}$$

$$H_2(\kappa) = H_0(\kappa)e^{+j\kappa\lambda/8} \quad . \tag{5b}$$

The dual-array obtained from the one depicted in Fig. 1 is schematically shown in Fig. 5 together with its spatial distribution, $h_1(x)$ and $h_2(x)$, derived from $h_0(x)$. The absolute value of its spectrum is the same as the one presented in Fig. 1(c).

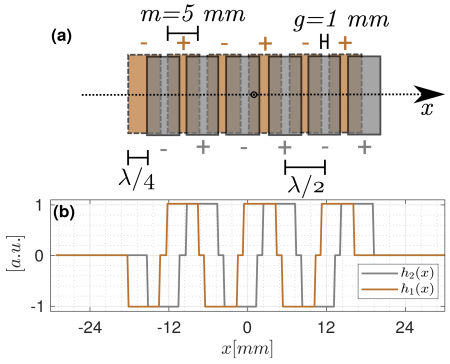

Figure 5: Schematic representation of a dual-array transducer (a) composed of two quarter-wavelength shifted single array where each one consists of 3 periods of alternate polarity (pulse and minus signs) elements with active length $m = 5$ mm and the gap between elements $g = 1$ mm, thus providing a $\lambda = 12$ mm spatial period. Ideal transducer spatial profiles (b). The first and second arrays are respectively represented by copper-colour and grey rectangles. The same colour is used to represent their spatial profiles.

It is considered here that the two arrays can be respectively excited by the two different signals, $g_1(t)$ and $g_2(t)$, whose Fourier transforms give their frequency distribution:

$$G_1(\omega) = \mathscr{F}\left\{g_1(t)\right\} \quad , \tag{6a}$$

$$G_2(\omega) = \mathscr{F}\left\{g_2(t)\right\} \quad . \tag{6b}$$

Therefore, each array gives rise to an individual operating region, defined by the product of their

respective temporal and spatial spectra:

$$S_1(\omega,\kappa) = G_1(\omega)H_1(\kappa) \quad , \tag{7a}$$

$$S_2(\omega,\kappa) = G_2(\omega)H_2(\kappa) \quad . \tag{7b}$$

The operating region of the dual array is then obtained by the superposition of the single-array operating regions:

$$\begin{aligned} S(\omega,\kappa) &= S_1(\omega,\kappa) + S_2(\omega,\kappa) = \\ &= [G_1(\omega)H_1(\kappa) + G_2(\omega)H_2(\kappa)] \\ &= \left[G_1(\omega)e^{-j\kappa\lambda/8} + G_2(\omega)e^{+j\kappa\lambda/8}\right] H_0(\kappa) \quad , \end{aligned} \tag{8}$$

where the last equality comes from Eq. 5. The choice of $g_1(t)$ and $g_2(t)$ acting over $h_1(x)$ and $h_2(x)$ can make $S(\omega,\kappa)$ non-symmetrical with respect to the κ-axis, therefore, enhancing the waves generated to one side with respect to the opposite side. This is the principle for designing excitation pulses that optimise unidirectional generation in this paper.

3. Design of optimal excitation methods for dual-array transducers

In this section, we analyse how time-delayed excitation signals provide either perfect constructive or destructive interferences for non-dispersive waves, but are not optimal for dispersive waves. Then, we propose new excitation methods that facilitate optimal constructive or destructive interferences for dispersive wave modes. The analysis is based on the resultant operation region obtained with each pair of excitation signals, and how they make it non-symmetric with respect to the κ-axis.

3.1. Time-delayed excitation methods

The most straightforward way to attempt unidirectional generation with a dual-array transducer is to delay the excitation signal that is applied to the second array in the same amount as the time it takes for the wave generated from each element of the first array to arrive at the respective element of the second array, as has been used extensively previously [7, 15, 23–27]. This way, the two sets of waves generated by each array propagate in-phase to the right of the dual-array, positive x-axis, producing ideal constructive interference for the forward propagating waves. Since the separation of the arrays is $\lambda/4$, this leads to a time delay of $\lambda/4c$, where c is the phase speed

of the wave of interest. Considering that the centre frequency of the excitation pulse, $1/T$, with T being its time-period, is set to match the dispersion relationship of the wave of interest, given by $c = \lambda/T$, then the time shift equals a quarter-period, $T/4$ [26]. This method is referred to as time-delay, or TD, hereinafter.

In order to address the effect of using the aforementioned time-delayed signal in the frequency-wavenumber spectrum, one needs to calculate the resultant operating region. Signals $g_1(t)$ and $g_2(t)$ are formally represented in the time and frequency domains by

$$g_1(t) = g_0(t) \longleftrightarrow G_1(\omega) = G_0(\omega) \quad , \tag{9a}$$

$$g_2(t) = g_0(t - T/4) \longleftrightarrow G_2(\omega) = e^{-j\omega T/4} G_0(\omega) \quad . \tag{9b}$$

Applying Eq. 9 into Eq. 8, with some manipulation, leads to

$$S(\omega, \kappa) = 2G_0(\omega) H_0(\kappa) e^{-j\omega T/8} cos\left(\frac{\omega T - \kappa\lambda}{8}\right) \quad , \tag{10}$$

showing that $S(\omega, \kappa)$ is maximum whenever the argument of the cosine is a multiple of π and minimum when it is an odd multiple of $\pi/2$. In particular, the first maximum and minimum loci in the κ-ω plane occur, respectively, at $\kappa\lambda = \omega T$ and $\kappa\lambda = \omega T - 4\pi$. Note that, at the centre frequency, $\omega = 2\pi/T$, the maximum and minimum loci lie at the nominal wavenumber of forward propagating wave, $\kappa = 2\pi/\lambda$, and backward propagating wave, $\kappa = -2\pi/\lambda$, respectively. This means that, for monochromatic driving signals, simultaneous ideal constructive interference in the forward direction and destructive interference in the backward direction occur. For the most practical case of finite-length pulses, which present a frequency bandwidth, this method, however, only ensures ideal constructive interference.

Following the same reasoning, if one delays the wave generated by the first array in the exact amount as the propagation time from the second array to the first, and further inverts the signal, i.e., multiply it by -1, then the waves generated by both arrays propagate to the left-hand side perfectly aligned but completely out-of-phase, thus producing a perfect destructive interference to the left-hand side. Formally, one has

$$g_1(t) = -g_0(t - T/4) \longleftrightarrow G_1(\omega) = -e^{-j\omega T/4} G_0(\omega) \quad , \tag{11a}$$

$$g_2(t) = g_0(t) \longleftrightarrow G_2(\omega) = G_0(\omega) \quad . \tag{11b}$$

This method is referred to as time-delay and inverse method, or TDI, hereinafter. Applying Eq. 11 into Eq. 8, with some manipulation, leads to

$$S(\omega,\kappa) = 2G_0(\omega)H_0(\kappa)e^{-j(\omega T/8-\pi/2)}sin\left(\frac{\omega T+\kappa\lambda}{8}\right) \quad . \tag{12}$$

In this case, the maximum and minimum occur at $\kappa\lambda = -\omega T + 4\pi$ and $\kappa\lambda = -\omega T$, respectively.

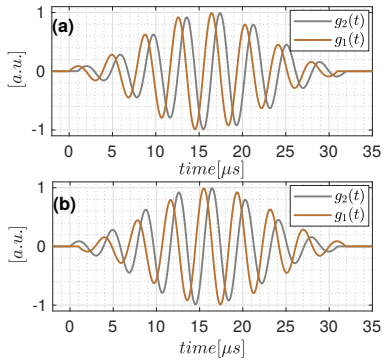

Figure 6: Excitation signals to unidirectionally generate the non-dispersive SH0 mode through the time-delay (TD) (a) and time-delay and inverse (TDI) (b) methods. The base signal, $g_0(t)$, is an 8-cycle tone-burst centred at 258.3kHz modulated by a Hamming window (shown in Fig. 2). Since the generated wave is non-dispersive, (a) and (b) also correspond to the synthetic propagated (SP) and synthetic propagated and inverse (SPI) excitation signals, respectively.

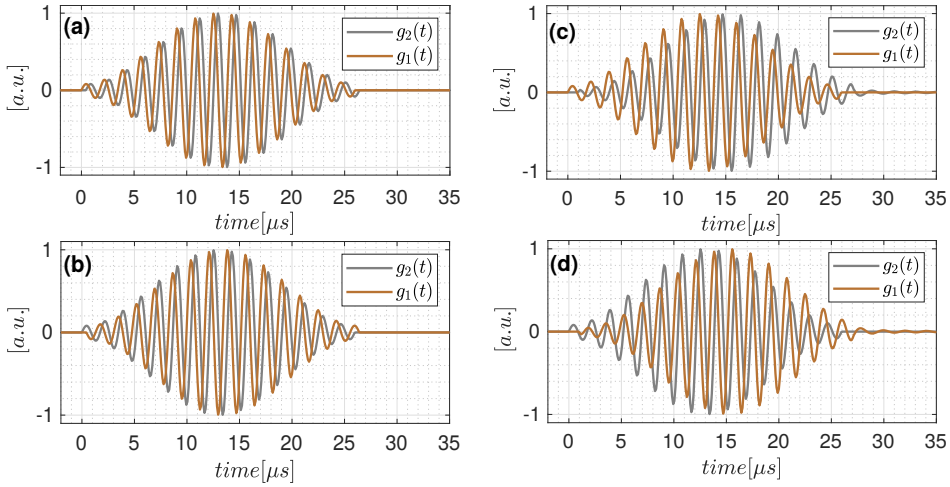

Figure 7: Excitation signals to unidirectionally generate the dispersive SH1 mode through the time-delay (TD) (a), time-delay and inverse (TDI) (b), synthetic propagated (SP) (c) and synthetic propagated and inverse (SPI) (d) methods. The base signal, $g_0(t)$, is a 15-cycle tone-burst centred at 577.7kHz modulated by a Hamming window (shown in Fig. 3).

Fig. 6(a) and Fig. 7(a) show the time-delayed excitation signals pairs where the base signal, $g_0(t)$, is the signals shown in Figs. 2 and 3, respectively. The respective time-delayed and inverse

excitation signals' pairs are shown in Fig. 6(b) and Fig. 7(b). Figs. 8(a) and 9(a) illustrate the operating region, $S(\omega, \kappa)$, for the TD and TDI methods, respectively, computed through Eqs. 10 and 12, when generating a non-dispersive wave. The maximum and minimum loci, blue and red lines, respectively, are superposed to it. Note that there is a trough in $S(\omega, \kappa)$ along the red line, whereas it is maximum along the blue line. The dispersion curve of the wave mode of interest is also superposed to $S(\omega, \kappa)$, black dash-dotted lines. Note that in Figs. 8(a) the maximum line coincides with the dispersion curve of forward propagating wave, providing theoretical perfect constructive interference for all the frequency range for forward propagating wave. The minimum line, however, is slanted concurrently to the dispersion curve of a backward propagating wave, thus providing destructive interference only at the centre frequency. Nevertheless, the absolute value of the operating region along the dispersion curve for negative wave numbers is considerably lower than for positive wavenumber. Meaning that forward propagating waves are enhanced whilst backward ones are weakened, despite being non-zero. In Figs. 9(a) the slope of maximum and minimum lines are now interchanged relative to Figs. 8(a). This means that the TDI is able to provide ideal destructive interference for backward propagated waves. Note that the operating region does not overlap the dispersion curve of the backward propagating wave since there is now a trough in it exactly along the dispersion curve. In this case, the backward propagating wave should be theoretically nullified, whereas the forward propagation wave still has high amplitude.

Figs. 8(b) and 9(b), correspond to the operating region when the excitation signal pair are the ones shown in Figs. 7(a) and (b), respectively, whose centre frequency is set to generate a dispersive wave. In this case, neither constructive nor destructive interferences occur all along the dispersion curves, since the dispersion curve is no longer a straight line. Despite TDI providing a trough in $S(\omega, \kappa)$ sloped to the same side as the dispersion curve for $\kappa < 0$, the latter still crosses non-zero portions of $S(\omega, \kappa)$. Therefore, the resultant wave that propagates to the weakened side is non-zero.

3.2. Synthetic propagated excitation methods

Following the same signal design reasoning, in order to produce ideally perfect constructive or destructive interferences for dispersive waves, one should apply to one array a signal that is equal to the wave that arrives at it, having departed from the other array. However, the propagation of a dispersive wave does not behave like a merely time shift, because each frequency component that composes the excitation pulse present a different phase speed. It can, nevertheless, be modelled by the propagating operator in the frequency domain: $e^{-j\kappa_n(\omega)\ell}$ [32, 33], where ℓ is the propagating

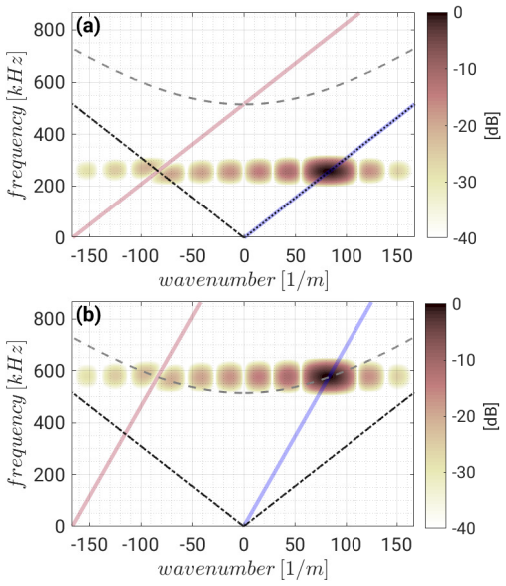

Figure 8: Operating region (colour plot) of the dual-array transducer driven by the time-delay (TD) method when the base signal is centred (a) at 258.3 kHz (shown in Fig. 2) and (b) at 577.7 kHz (shown in Fig. 3) The blue and red lines indicate the loci of maxima and minima interference, respectively. The black dash-dotted line indicates the dispersion curve of the non-dispersive SH0 mode, and the grey dashed line is the dispersion curve of the dispersive SH1 mode.

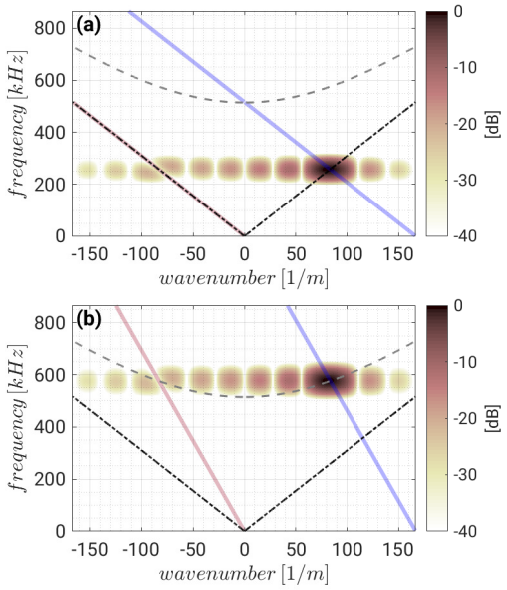

Figure 9: Operating region (colour plot) of the dual-array transducer driven by the time-delay and inverse (TDI) method when the base signal is centred (a) at 258.3 kHz (shown in Fig. 2) and (b) at 577.7 kHz (shown in Fig. 3) The blue and red lines indicate the loci of maxima and minima interference, respectively. The black dash-dotted line indicates the dispersion curve of the non-dispersive SH0 mode, and the grey dashed line is the dispersion curve of the dispersive SH1 mode.

distance and $\kappa_n(\omega)$ is the frequency-dependent wavenumber expression for wave n, with n being an index that identifies the wave of interest.

Therefore, if one excites the second array with a signal that is identical to the wave that arrives at its position departing from the first array, one achieves theoretically perfect constructive interference. This is formally represented by adopting the following excitation signals:

$$g_1(t) = g_0(t) \longleftrightarrow G_1(\omega) = G_0(\omega) \quad , \tag{13a}$$

$$g_2(t) = \mathscr{F}^{-1}\left\{e^{-j\kappa_n(\omega)\lambda/4} G_0(\omega)\right\} \longleftrightarrow G_2(\omega) = e^{-j\kappa_n(\omega)\lambda/4} G_0(\omega) \quad , \tag{13b}$$

where Eq. 13b can be understood as a synthetically propagated signal from the first to the second array, where arrays are separated by a quarter-wavelength $\ell = \lambda/4$. This method is referred to as synthetic propagated method, or SP, hereinafter. Note that there is, in principle, no closed-form

equation for the time-domain signal $g_2(t)$. One should calculate it by the inverse Fourier transform, $\mathscr{F}^{-1}$, of its spectrum, obtained from phase-shifting $G_0(\omega)$.

With Eq. 13, Eq. 8 becomes

$$S(\omega,\kappa) = 2G_0(\omega)H_0(\kappa)e^{-j\kappa_n(\omega)\lambda/8}cos\left(\frac{\kappa_n(\omega)\lambda - \kappa\lambda}{8}\right) \quad . \tag{14}$$

A maximum locus occurs, now, for $\kappa = \kappa_n(\omega)$ and a minimum lies at $\kappa = \kappa_n(\omega) - 4\pi/\lambda$, meaning that constructive interference is ideally obtained for wave mode n, regardless of its dispersive nature. Note that, if mode n is non-dispersive, then $\kappa_n(\omega) = \omega T/\lambda$, which means that the propagating operator corresponds to a merely time-shift and Eqs. 13 and 14 are equivalent to Eq. 9 and 10, respectively. Fig. 7(c) illustrates the synthetic propagated signal to generate a dispersive wave. Note that the latter considerably differs from the simpler time-delayed signal, shown in Fig. 7(a). For instance, note that it presents a long oscillating tail for later times. The synthetic propagated signal used to generate the non-dispersive mode is identical to the time-delayed version, shown in Fig. 6(a). Fig. 10 shows $S(\omega,\kappa)$ in this case. As can be seen, the locus of constructive interference coincides with the forward propagating dispersion curves either for dispersive or non-dispersive waves.

Finally, using a similar approach to the TDI method, one can excite the first array with a synthetically propagated signal from the second array which is multiplied by -1, in order to ensure destructive interference for a dispersive wave. This method is referred to as synthetic propagated and inverse method, or SPI, hereinafter. The excitation signals should then be

$$g_1(t) = -\mathscr{F}^{-1}\left\{e^{-j\kappa_n(\omega)\lambda/4}G_0(\omega)\right\} \longleftrightarrow G_1(\omega) = -e^{-j\kappa_n(\omega)\lambda/4}G_0(\omega) \quad , \tag{15a}$$

$$g_2(t) = g_0(t) \longleftrightarrow G_2(\omega) = G_0(\omega) \quad , \tag{15b}$$

and Eq. 8 becomes

$$S(\omega,\kappa) = 2G_0(\omega)H_0(\kappa)e^{-j(\kappa_n(\omega)\lambda/8-\pi/2)}sin\left(\frac{\kappa_n(\omega)\lambda + \kappa\lambda}{8}\right) \quad . \tag{16}$$

In this case, a minimum locus occurs, for $\kappa = -\kappa_n(\omega)$ and a maximum lies at $\kappa = -\kappa_n(\omega) + 4\pi/\lambda$, meaning that destructive interference is obtained for wave mode n at all frequencies. Fig. 7(d) illustrates the synthesized synthetic propagated and inverse signal to generate a dispersive wave. As shown in Fig. 11, the minimum locus follows the backward travelling dispersion curves, enforcing a trough for all the frequencies, and then ideally producing identically null signals for the backward propagated wave, regardless of the dispersive nature of the wave.

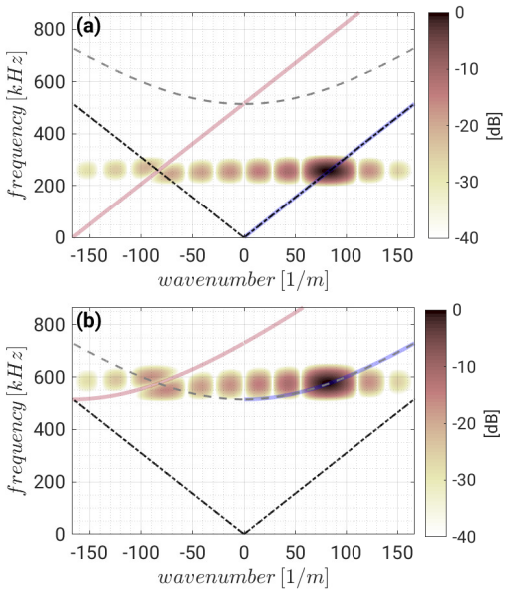

Figure 10: Operating region (colour plot) of the dual-array transducer driven by the synthetic propagated (SP) method when the base signal is (a) at 258.3 kHz (shown in Fig. 2) and (b) at 577.7 kHz (shown in Fig. 3) The blue and red lines indicate the loci of maxima and minima interference, respectively. The black dash-dotted line indicates the dispersion curve of the non-dispersive SH0 mode, and the grey dashed line is the dispersion curve of the dispersive SH1 mode.

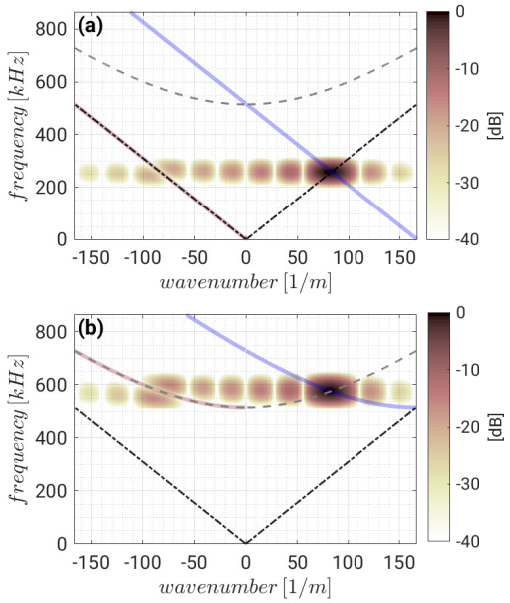

Figure 11: Operating region (colour plot) of the dual-array transducer driven by the synthetic propagated and inverse (SPI) method when the base signal is centred (a) at 258.3 kHz (shown in Fig. 2) and (b) at 577.7 kHz (shown in Fig. 3) The blue and red lines indicate the loci of maxima and minima interference, respectively. The black dash-dotted line indicates the dispersion curve of the non-dispersive SH0 mode, and the grey dashed line is the dispersion curve of the dispersive SH1 mode.

It is worth highlighting the differences between the designing procedures to obtain the excitation signals with the time-delayed based, namely, TD and TDI, and synthetic propagated based, namely, SP and SPI, methods. For the former, the centre frequency of the base signal, $g_0(t)$, is defined through the dispersion curve of the wave mode of interest and the nominal wavelength of the dual-array transducer. Then, this signal is time-delayed, in the time domain, through the left-hand side of Eq. 9 or Eq. 11, for the TD or TDI methods, respectively, in order to obtain the final excitation signals pairs, namely, $g_1(t)$ and $g_2(t)$. For the latter, the centre frequency of $g_0(t)$ is also determined through the dispersion curve of the wave mode of interest, but its frequency spectrum, $G_0(\omega)$, has to be computed, as per Eq. 2, prior to obtaining the final excitation signals pairs. Then, $G_1(\omega)$ and $G_2(\omega)$ are computed, in the frequency domain, through the frequency-dependent phase-shift according to the dispersion curve of the wave mode of interest, as expressed in the right-hand side of Eq. 13 or Eq. 15, for the SP or SPI methods, respectively. Finally, the time domain excitation signals, $g_1(t)$

and $g_2(t)$, that are to be applied to the dual-array transducer, are computed through the inverse Fourier transform, of their respective spectra.

It is also worth mentioning that one-dimensional source spatial distributions, $h_1(x)$ and $h_2(x)$, were considered here in order to devise the aforementioned methods in the frequency-wavenumber domain. Clearly, real transducers present finite width and their spatial distribution is not a one-dimension function. The one-dimension simplification is, nevertheless, a good approximation for most guided waves problems when one is interested in the wavefield along the main beam axis [5, 17], i.e at 0^o and 180^o angles from the transducer longitudinal centreline, where the interference mechanism exploited herein holds. Furthermore, the radiated beam is usually mostly concentrated in the transducer longitudinal centreline axis, where suppression of the backward generated wave plays a crucial role in unidirectional generation. Generally, the wider the transducer, the more concentrated is its main beam [34]. This also holds for dual-array transducers but the exact radiation diagram for lateral angles depends on the dual-array geometry [26, 35].

4. SH guided waves generated by dual PPM EMAT

Shear-horizontal ultrasonic guided waves in flat, parallel faced plates are polarized in the z-direction whilst propagating in the x-direction, where the plate surfaces lie in the x-z plane. There are an infinite number of SH wave modes, the dispersion relationship of mode n is given by [36]

$$\kappa_n(\omega) = \pm\sqrt{\omega^2/c_T^2 - n^2\pi^2/h^2} \quad , \tag{17}$$

where h is the plate thickness and c_T is the bulk shear-wave speed in the medium. A positive wavenumber stands for forward propagating SH wave, whereas a negative one for backward propagating waves. The zero-order mode ($n = 0$), or the SH0 mode, is non-dispersive on flat plates, with wavenumber equal to $\kappa_0(\omega) = \omega/c_T$ or a constant phase speed equal to $c = c_T$. All other modes are dispersive, meaning that the wavenumber does not depend linearly on the frequency, or their phase speed is not constant. In order to generate SH waves, one has to impose shear stress parallel to the plate surface and perpendicular to the propagation direction.

SH waves can be efficiently generated with PPM EMATs, which consist of an alternate-polarity magnet array with a racetrack coil underneath [37]. EMATs induce Lorentz forces in a conductive medium, given by the cross product $\mathbf{F} = \mathbf{J} \times \mathbf{B}$, where $\mathbf{J}$ is the induced electric current density which can be considered to act effectively at the surface of the sample due to the small skin-depth, and generally with opposite direction of the current flowing in the coil, and $\mathbf{B}$ is the magnet field from

the magnets [28]. Due to the alternating polarity of the magnets, an array of z-polarized forces, capable of generating SH ultrasonic waves arises in the surface of the medium, which determines the spatial distribution of the array, $h_0(x)$. The current injected into the coil determines the temporal dependence, $g_0(t)$, of the forces for this spatial force distribution.

The dual-array transducer used here is schematically shown in Fig. 12. It consists of two PPM-like EMATs, where one array is side-shifted (z-direction) relative to the other, in order to accommodate both sets of forces; the second array is then longitudinally shifted (x-direction) by a quarter-wavelength [25]. In Fig. 12, each red or magenta square represents a magnet oriented with its north pole towards the positive y-direction, whereas blue or cyan squares represent a magnet oriented with its south pole towards the negative direction. Blue and red magnets are related to the first array, whereas cyan and magenta to the second array. Thus, forces from each array follow the grey and copper-colour arrows in Fig. 12. The magnets' length of each element of the array is $m = 5$ mm and the gap between elements of the same array is $g = 1$ mm, thus producing a nominal wavelength of $\lambda = 12$ mm, with both arrays longitudinally shifted by $\lambda/4$. Assuming a small lift-off between the magnet arrays and the sample surface, the induced forces distribution can be considered homogeneously distributed in the area underneath each magnet [5, 34]. Therefore, along the x-axis, which coincides with the longitudinal centreline of the dual-array, one can assume that the spatial distributions, $h_1(x)$ and $h_2(x)$, are the ones depicted in Fig. 5(b).

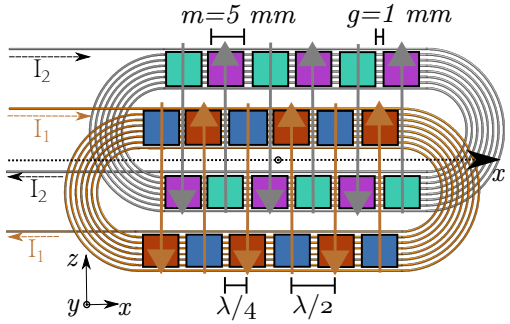

Figure 12: Side-shifted dual PPM EMAT array with dimensions. Red and blue rectangles represent north and south magnets poles, respectively, of the first array and magenta and cyan rectangles, north and south magnets poles, respectively, of the second array. The second array is longitudinally shifted from the first by a quarter-wavelength. Underneath each array, a racetrack coil is placed, here presented by copper-colour and grey wire coils, respectively, into which currents I_1 and I_2 are respectively injected, represented by the dashed arrows. Two sets of Lorentz forces thus arise, schematically represented by the copper-colour and grey continuous arrows. The x-axis is located in the middle of the dual-array, along its centreline, represented by the dotted line.

5. Experimental validation

The excitation signals, given by Eqs. 9, 11, 13 or 15, were calculated in a computer and transferred to a two-channel arbitrary signal generator, in order to synthesize them. Next, the synthesized signals were power amplified and then connected to each coil of the dual array transducer, which was positioned in the middle of a 3 mm thick, 1 m long, aluminium plate. Two commercial conventional PPM EMATs from Sonemat Ltd. were used as receivers, positioned 250 mm from the centre of the transmitter, either at its left- or right-hand side, in order to capture the generated waves, the former is the weakened side and the latter, the enhanced side. Fig. 13 schematically shows the experimental setup.

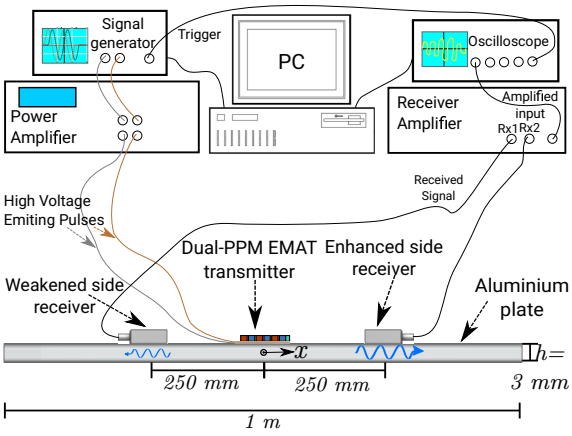

Figure 13: Experimental setup.

In order to generate the non-dispersive SH0 mode whose phase speed equals the bulk shear wave speed, c_T = 3100 m/s, at λ = 12 mm nominal wavelength of the transducer, a base signal $g_0(t)$, composed of an 8-cycle tone-burst centred at 258.3 kHz, modulated by a Hamming window was used, as shown in Fig. 2. The current excitation signals for the first and second arrays to unidirectionally generate the non-dispersive SH0 mode through the TD and TDI methods, Eqs. 9 and 11, respectively, are shown in Fig. 6(a) and (b), respectively. The operation region, $S(\omega, \kappa)$, formed by the transducer spatial distribution and each pair of excitation of signals are shown in Figs. 8(a) and 9(a), respectively, together with the dispersion curve of the SH0 mode. Recall that, since SH0 is non-dispersive, the SP and SPI methods provide the same excitation signals as the TD and TDI methods, respectively.

The experimental received signals for each excitation signal is shown in Fig. 14. Fig. 14(a) shows a low-amplitude signal, since destructive interference occurs only at the centre frequency of the

pulse. Fig. 14(b) shows that the trough in the operation region coinciding with the SH0 dispersion curve, obtained with the TDI method, produces a virtually nullified backwards propagated wave.

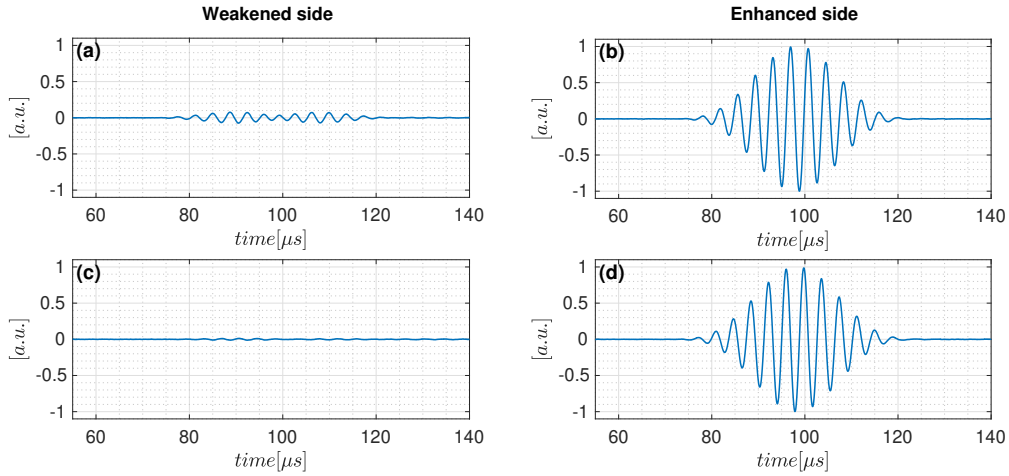

Figure 14: Experimental received SH0 waveforms at the weakened side (a) and (c), and at the enhanced side (b) and (d), due to unidirectional generation of the non-dispersive SH0 mode through the time-delay (TD) (a) and (b), and time-delay and inverse (TDI) (c) and (d), methods.

The effectiveness of unidirectional generation can be assessed by the forward to backward wave ratio (FBWR), defined by the ratio of the peak-to-peak amplitude of the forward generated wave to the peak-to-peak amplitude of the backwards generated wave. This value is reported in Table 1, in dB, together with the peak-to-peak amplitude of the forward generated wave, normalized per the maximum value, obtained with both methods used for generating the SH0 mode. As it can be seen, the TDI considerably increases FBWR, by about 15 dB. The effect of an ideal perfect constructive interference, produced by the TD method, is a negligible amplitude increase of the forward propagated wave.

The dispersive SH1 mode was also unidirectionally generated using the aforementioned methods. A 15-cycle tone-burst centred at $577.7kHz$ modulated by a Hamming window was used as $g_0(t)$, as shown in Fig. 3. The centre frequency was chosen to match its mode dispersion curve at the $\lambda = 12$ mm nominal wavelength, and more temporal cycles, compared to the SH0 excitation, were used to narrow the frequency spectrum and ensure single-mode generation. The excitation signals for the four methods are shown in Fig. 7. SP and SPI methods used the theoretical wavenumber expression, $\kappa_1(\omega)$, given by Eq. 17, in order to compute the excitation signals through Eqs. 13 and 15, respectively. The operation regions, together with the dispersion curve of the SH1 mode, are shown in Figs. 8(b), 9(b), 10(b) and 11(b).

Table 1: Experimental forward to backward wave ratio (FBWR) and normalized peak-to-peak amplitude of the forward generated wave for the non-dispersive SH0 and dispersive SH1 mode. For the generation of the non-dispersive SH0 mode, methods SP and TD are equivalent, as well as SPI and TDI, and thus only values for TD and TDI are presented.

	FBWR (dB)		Peak-to-peak Fwd. (norm.)	
Method	SH0	SH1	SH0	SH1
TD	22.4	12.3	1	0.999
TDI	37.7	15.7	0.999	0.997
SP	—	08.4	—	1
SPI	—	29.5	—	0.990

The experimentally received signals for each excitation method are shown in Fig. 15, and the values for FBWR and amplitude of the forward propagated wave, normalized per the maximum value obtained amongst the four methods used for generating the SH1 mode, are reported in Table 1. Note that the ideal constructive interference provided by the SP method indeed shows the highest amplitude forward propagated wave, which is very slightly increased compared to the other methods, but the destructive interference is considerably compromised, being the one that provided the worse wave cancellation to the backward direction. Interestingly, even the simplest TD method showed about 4 dB higher FBWR than the SP method. This happens because the backward propagating wave crosses several non-negligible amplitude portions of the operating region, as can be seen in Fig. 10(b). When compared to the operating region of the TD method, in Fig. 8(b), one can see that the trough produced by the former at the negative κ-axis differs from the latter in such a way that makes the dispersion curve of the SH1 mode, dashed grey line, cross longer regions of the operating regions with high amplitude for the SP method. On the other hand, the SPI method shows excellent performance, producing virtually zero backwards generated wave, with an amplitude that is approximately 30 dB lower than the forward wave, and just 1% lower amplitude to the enhanced side. It is worth highlighting that, since the SH1 mode is dispersive, TDI is unable to provide this level of wave cancellation to the backward travelling wave, and the more sophisticated excitation signal pair, provided by the SPI method proposed here is required.

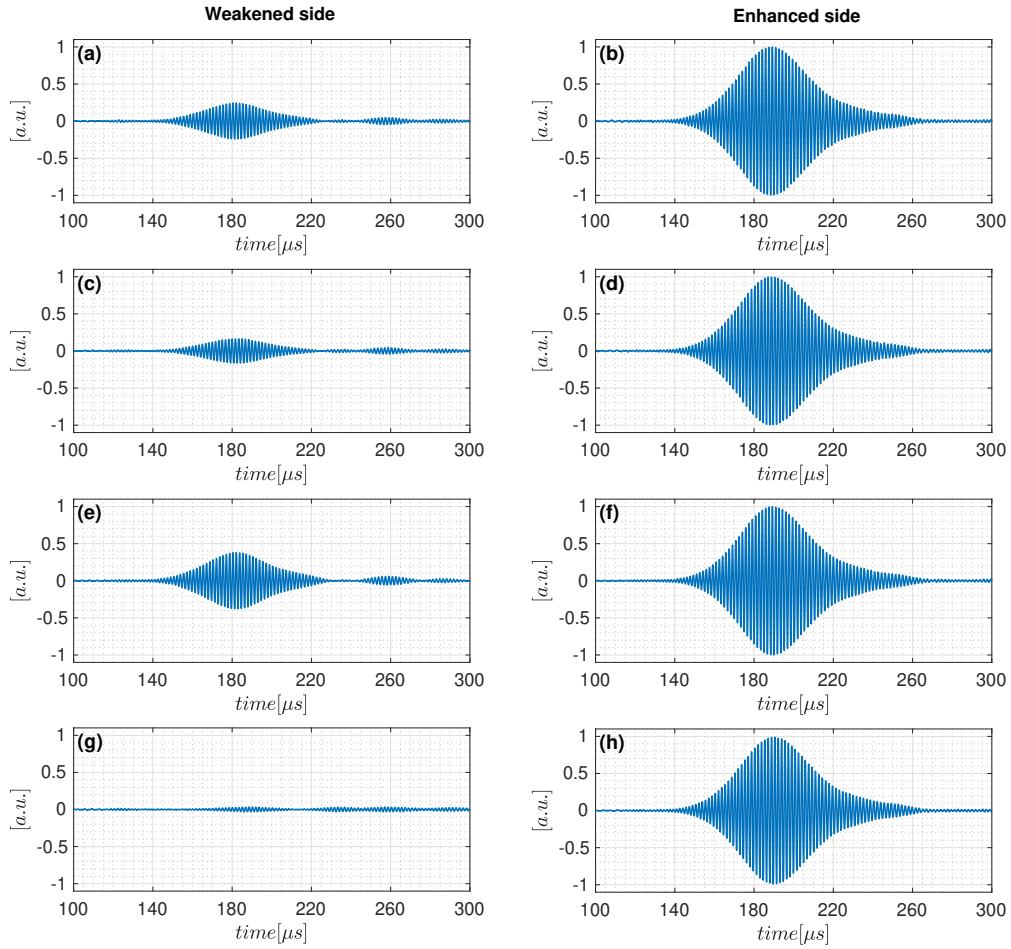

Figure 15: Experimental received SH1 waveforms at the weakened side (a), (c), (e) and (g), and at the enhanced side (b), (d), (f) and (g) due to unidirectional generation of the dispersive SH1 mode through the time-delay (TD) (a) and (b), time-delay and inverse (TDI) (c) and (d), synthetic propagated (SP) (e) and (f) and synthetic propagated and inverse (SPI) (g) and (h), methods.

6. Conclusion

The theoretical frequency-wavenumber spectrum for dual-array transducers was derived, based on the joint spectra of the excitation pulses and the ideal transducer spatial distributions. Depending on the excitation signals applied to drive each array, the operation frequency can be non-symmetrical relative to the wavenumber axis, meaning that the forward and backward propagating waves are generated unequally. Careful design of the excitation signals applied to drive each array can produce minima and maxima loci in the frequency-wavenumber pair that allow perfect constructive or destructive interference for forward and backwards generated waves, allowing one to design optimal excitation signals.

Two conventional driving methods that generate waves in a single direction, which have been proposed previously, were investigated in the frequency-wavenumber domain. The first method simply uses a time-shifted pulse into one array relative to the other; the second further inverts the time-shifted pulse. Both theoretical calculation and the experimental results demonstrated that they produce ideally perfect constructive or destructive interferences, respectively, for non-dispersive waves. They are, however, less effective for unidirectional generation of dispersive waves.

Consequently, two new driving methods, namely, synthetic propagated (SP) and synthetic propagated and inverse (SPI), were proposed. They use synthetic propagated signals, instead of simple time-shifted signals, with SP and SPI producing optimal constructive or destructive interferences, respectively, for dispersive and non-dispersive wave modes. When operated on non-dispersive wave modes, they are equivalent to the time-shift based methods. The SPI method provides ideal perfect destructive interference even for highly dispersive waves, showing great potential for unidirectional generation of different types of waves.

The conventional methods, together with our proposed methods, were evaluated here for unidirectional generation of ultrasonic shear horizontal guided waves modes generated by a dual PPM array EMAT. Both the non-dispersive fundamental SH0 mode and the first-order dispersive SH1 mode were used, with experimental results agreeing well with the theoretical frequency-wavenumber spectrum behaviour. The SP method provides ideal constructive interference for the forward propagated wave, and thus produced a slight amplitude increase in the forward direction, but up to approximately 20 dB worse unidirectionality than the SPI method, which provides ideal destructive interference to the backward direction. Unidirectional generation using the SPI method allowed one to experimentally generate the dispersive SH1 wave mode with about 30 dB unidirectionality, since the operating region is theoretically null along the dispersion curves of backward travelling waves.

Acknowledgments

This study was financed in part by the Coordenação de Aperfeiçoamento de Pessoal de Nível Superior - Brasil (CAPES) - Finance Code 001, and by the Carlos Chagas Filho Foundation for Research Support of Rio de Janeiro State (FAPERJ).

References

[1] A. Mamishev, K. Sundara-Rajan, F. Yang, Y. Du, M. Zahn, Interdigital sensors and transducers, Proceedings of the IEEE 92 (5) (2004) 808–845.

[2] A. Bulletti, P. Giannelli, M. Calzolai, L. Capineri, Multielement interdigital transducers for structural health monitoring, in: 2018 IEEE International Ultrasonics Symposium (IUS), 2018, pp. 1–3.

[3] W. Zhu, J. Rose, Lamb wave generation and reception with time-delay periodic linear arrays: a bem simulation and experimental study, IEEE Transactions on Ultrasonics, Ferroelectrics, and Frequency Control 46 (3) (1999) 654–664.

[4] J. Li, J. Rose, Implementing guided wave mode control by use of a phased transducer array, IEEE Transactions on Ultrasonics, Ferroelectrics, and Frequency Control 48 (3) (2001) 761–768.

[5] L. Xiang, D. Greenshields, S. Dixon, R. S. Edwards, Phased electromagnetic acoustic transducer array for rayleigh wave surface defect detection, IEEE Transactions on Ultrasonics, Ferroelectrics, and Frequency Control 67 (7) (2020) 1403–1411.

[6] P. Petcher, S. Burrows, S. Dixon, Shear horizontal (SH) ultrasound wave propagation around smooth corners, Ultrasonics 54 (4) (2014) 997 – 1004.

[7] M. Chen, Q. Huan, F. Li, A unidirectional SH wave transducer based on phase-controlled antiparallel thickness-shear (d15) piezoelectric strips, Theoretical and Applied Mechanics Letters 10 (5) (2020) 299–306.

[8] H. Qiu, M. Chen, F. Li, Selective excitation of high-order shear horizontal wave (SH1) by using a piezoelectric interdigital transducer, Mechanical Systems and Signal Processing 165 (2022) 108390.

[9] W. Zhu, A finite element analysis of the time-delay periodic ring arrays for guided wave generation and reception in hollow cylinders, IEEE Transactions on Ultrasonics, Ferroelectrics, and Frequency Control 48 (5) (2001) 1462–1470.

[10] X. Niu, W. Duan, H.-P. Chen, H. Marques, Excitation and propagation of torsional t(0,1) mode for guided wave testing of pipeline integrity, Measurement 131 (2019) 341–348.

[11] B. W. Drinkwater, P. D. Wilcox, Ultrasonic arrays for non-destructive evaluation: A review, NDT & E Int. 39 (7) (2006) 525–541.

[12] P. Malinowski, T. Wandowski, I. Trendafilova, W. Ostachowicz, A phased array-based method for damage detection and localization in thin plates, Structural Health Monitoring 8 (1) (2009) 5–15.

[13] Q. Huan, M. Chen, Z. Su, F. Li, A high-resolution structural health monitoring system based on SH wave piezoelectric transducers phased array, Ultrasonics 97 (2019) 29–37.

[14] J. Tkocz, D. Greenshields, S. Dixon, High power phased emat arrays for nondestructive testing of as-cast steel, NDT & E Int. 102 (2019) 47–55.

[15] S. Wang, R. Su, X. Chen, L. Kang, G. Zhai, Numerical and experimental analysis of unidirectional meander-line coil electromagnetic acoustic transducers, IEEE Transactions on Ultrasonics, Ferroelectrics, and Frequency Control 60 (12) (2013) 2657–2664.

[16] G. Zhai, T. Jiang, L. Kang, Analysis of multiple wavelengths of lamb waves generated by meander-line coil emats, Ultrasonics 54 (2) (2014) 632–636.

[17] G. Zhai, Y. Li, Y. Qin, Y. Liu, Design method of multiwavelength emats based on spatial domain harmonic control, IEEE Transactions on Ultrasonics, Ferroelectrics, and Frequency Control 68 (6) (2021) 2259–2270.

[18] S. Hill, S. Dixon, Frequency dependent directivity of periodic permanent magnet electromagnetic acoustic transducers, NDT & E Int. 62 (2014) 137–143.

[19] S. Dixon, P. A. Petcher, Y. Fan, D. Maisey, P. Nickolds, Ultrasonic metal sheet thickness measurement without prior wave speed calibration, Journal of Physics D: Applied Physics 46 (44) (2013) 445502.

[20] A. C. Kubrusly, J. P. von der Weid, S. Dixon, Experimental and numerical investigation of the interaction of the first four SH guided wave modes with symmetric and non-symmetric discontinuities in plates, NDT & E Int. 108 (2019) 102175.

[21] M. Tabatabaeipour, O. Trushkevych, G. Dobie, R. S. Edwards, R. McMillan, C. Macleod, R. O'Leary, S. Dixon, A. Gachagan, S. G. Pierce, Application of ultrasonic guided waves

to robotic occupancy grid mapping, Mechanical Systems and Signal Processing 163 (2022) 108151.

[22] M. Clough, M. Fleming, S. Dixon, Circumferential guided wave EMAT system for pipeline screening using shear horizontal ultrasound, NDT & E Int. 86 (2017) 20 – 27.

[23] T. Yamasaki, S. Tamai, M. Hirao, Arrayed-coil emat for longitudinal wave in steel wires, in: 1998 IEEE Ultrasonics Symposium. Proceedings (Cat. No. 98CH36102), Vol. 1, 1998, pp. 789–792 vol.1.

[24] X. Chen, R. Su, H. Zhang, S. Wang, G. Zhai, Influence of coil parameters on transduction performance of unidirectional emats for rayleigh wave, in: 2013 Far East Forum on Nondestructive Evaluation/Testing: New Technology and Application, 2013, pp. 150–154.

[25] A. C. Kubrusly, L. Kang, S. Dixon, Unidirectional shear horizontal wave generation with side-shifted periodic permanent magnets electromagnetic acoustic transducer, IEEE Transactions on Ultrasonics, Ferroelectrics, and Frequency Control 67 (12) (2020) 2757–2760.

[26] A. C. Kubrusly, L. Kang, I. Martins, S. Dixon, Unidirectional shear horizontal wave generation by periodic permanent magnets electromagnetic acoustic transducer with dual linear-coil array, IEEE Transactions on Ultrasonics, Ferroelectrics, and Frequency Control 68 (10) (2021) 3135–3142.

[27] K. Rieger, D. Erni, D. Rueter, Unidirectional emission and detection of lamb waves based on a powerful and compact coils-only emat, NDT & E Int. (2021) 102492.

[28] M. Hirao, O. H, EMATs for Science and Industry: Noncontacting Ultrasonic Measurements, Springer, 2017.

[29] G. S. Kino, Acoustic waves: devices, imaging, and analog signal processing, Prentice-Hall, 1987.

[30] F. J. Harris, On the use of windows for harmonic analysis with the discrete fourier transform, Proceedings of the IEEE 66 (1) (1978) 51–83.

[31] P. Khalili, F. Cegla, Excitation of single-mode shear-horizontal guided waves and evaluation of their sensitivity to very shallow crack-like defects, IEEE Transactions on Ultrasonics, Ferroelectrics, and Frequency Control 68 (3) (2021) 818–828.

[32] A. Roueff, J. Mars, J. Chanussot, H. Pedersen, Dispersion estimation from linear array data in the time-frequency plane, IEEE Transactions on Signal Processing 53 (10) (2005) 3738–3748.

[33] D. Hesse, P. Cawley, A single probe spatial averaging technique for guided waves and its application to surface wave rail inspection, IEEE Transactions on Ultrasonics, Ferroelectrics, and Frequency Control 54 (11) (2007) 2344–2356.

[34] O. V. Muraveva, V. V. Muravev, Y. V. Myshkin, Laws of formation of grating lobes in the acoustic field of electromagneticacoustic transducers as a linear array of unidirectional conductors, NDT & E Int. 93 (2018) 40–56.

[35] L. M. Martinho, A. C. Kubrusly, L. Kang, S. Dixon, Enhancement of the unidirectional radiation pattern of shear horizontal ultrasonic waves generated by side-shifted periodic permanent magnets electromagnetic acoustic transducers with multiple rows of magnets, IEEE Sensors Journal , early access (2022) 1–1.

[36] J. L. Rose, Ultrasonic Guided waves in solid media, Cambridge University Press, 2014.

[37] H. Miao, F. Li, Shear horizontal wave transducers for structural health monitoring and non-destructive testing: A review, Ultrasonics 114 (2021) 106355.